Qureshi et al. Nanoscale Research Letters (2016) 11:472
DOI 10.1186/s11671-016-1692-2

Nanoscale Research Letters

NANO EXPRESS Open Access

Heat and Mass Transfer Analysis of MHD Nanofluid Flow with Radiative Heat Effects in the Presence of Spherical Au-Metallic Nanoparticles

M. Zubair Akbar Qureshi[1], Qammar Rubbab[1*], Saadia Irshad[2], Salman Ahmad[3] and M. Aqeel[3]

Abstract

Energy generation is currently a serious concern in the progress of human civilization. In this regard, solar energy is considered as a significant source of renewable energy. The purpose of the study is to establish a thermal energy model in the presence of spherical Au-metallic nanoparticles. It is numerical work which studies unsteady magnetohydrodynamic (MHD) nanofluid flow through porous disks with heat and mass transfer aspects. Shaped factor of nanoparticles is investigated using small values of the permeable Reynolds number. In order to scrutinize variation of thermal radiation effects, a dimensionless Brinkman number is introduced. The results point out that heat transfer significantly escalates with the increase of Brinkman number. Partial differential equations that govern this study are reduced into nonlinear ordinary differential equations by means of similarity transformations. Then using a shooting technique, a numerical solution of these equations is constructed. Radiative effects on temperature and mass concentration are quite opposite. Heat transfer increases in the presence of spherical Au-metallic nanoparticles.

Keywords: Thermal radiation effects, Au-metallic nanoparticles, Viscous dissipation, Wall expansion ratio

Background

Today, solar thermal systems with nanoparticles have become a new area of investigation. Further thermal radiative transport has notable significance in several applications in the field of engineering such as solar power collectors, astrophysical flows, large open water reservoirs, cooling and heating chambers, and various other industrialized and environmental developments. Nanoparticles have an ability to absorb incident radiations. Bakier [1] explored how thermal radiation affects mixed convection from a vertical surface in a porous medium. Damseh [2] looked at effects of radiation heat transfer and transverse magnetic field in order to perform numerical analysis of magnetohydrodynamics-mixed convection. Hossain and Takhar [3] analyzed how radiation influences forced and free convection flow on issues related to heat transfer. In a study, Zahmatkesh [4] explored that temperature is almost uniformly distributed in the vertical sections inside an enclosure as a result of thermal radiation. The findings of this study concluded that the streamlines are almost parallel along the vertical walls. An analysis of thermal radiation in forced and free convection flow on an inclined flat surface was carried out by Moradi et al. [5]. In the same vein, Pal and Mondal [6] examined results of radiation on forced and free convection on a vertical plate set in a porous medium having variable porosity. Hayat et al. [7] extended thermal radiation results in magnetohydrodynamic (MHD) steady nanofluid flow through a rotating disk.

Nanofluids are a new dynamic sub-class of nanotechnology. This is the reason why the majority of scientists and researchers are persistently attempting to take a shot at novel elements of nanotechnology. Das and Choi [8] named the amalgamation of these particulate matters of particle size in the order of nanometers as a

* Correspondence: rubabqammar@gmail.com
[1]Department of Computer Science, Air University, Multan Campus, Islamabad, Pakistan
Full list of author information is available at the end of the article

Table 1 Thermophysical properties of water and metallic nanoparticles

	$\rho(Kgm^{-3})$	$C_p(JKg^{-1}K^{-1})$	$K(Wm^{-1}K^{-1})$
H_2O	997.1	4179	0.613
Au (metallic)	19,300	1290	318

"nanofluid." Nano-particulate suspension in a base fluid makes it superior and finer in terms of heat transfer compared to conventional fluids. Abrasion-related properties of nanofluids are found to be excellent over traditional fluid-solid mixtures. Metallic nanoparticles have vast applications in the ambit of nanosciences. Nanofluids with metallic nanoparticles have a lot of useful applications especially in the biological sciences. The photothermal metallic nanoblade is another novel methodology for delivering highly concentrated material into mammalian cells. Cryosurgery is used to destroy undesired tissues with penetration of metallic nanoparticles into the target tissues. Gold nanoparticles are the finest and most efficient drug-carrying molecules. The injection/suction factor with relaxing/contracting porous orthogonally moving disks in well-established flows is regarded as an important area of study in fluid mechanics. This area of study has attracted significant applications in engineering sciences, for example, crystal growth procedures, computer storage equipment, rotating machineries, viscometers, heat and mass exchangers, and lubricants [9–13]. Ashraf et al. [14] discussed non-Newtonian fluid flow in orthogonally moving coaxial porous and non-porous disks. Kashif et al. [15] conducted a ground-breaking study of nanofluid flow due to orthogonally porous moving disks. The core principles of magnetohydrodynamics flow are particularly used in spacecraft propulsion, plasma accelerators for ion thrusters, light ion beam, powered inertial confinement, MHD generators, pumps, bearing, and boundary layer flow in aerodynamics. Nikiforov [16] performed a seminal study on MHD flow. Various other analysts have also emphasized this idea, and points of interest are explored in various studies, for example, Hatami et al. [17, 18], Sheikholeslami et al. [19–26], Hayat et al. [27–29], Rashidi et al. [30], Mehrez et al. [31], Mabood et al. [32], Abbasi et al. [33], and Shehzad et al. [34].

Thermal radiation with viscous dissipation effects in nanofluid flow between porous orthogonally moving disks has to the best of our knowledge not been deliberated. Spherical Au-metallic nanoparticles are considered with a Hamilton–Crosser thermal conductivity model. In order to determine possible anomalous heat transfer enhancement related to spherical Au-metallic nanoparticles, volume fraction, velocity, temperature, and mass transport equations for permeability, Reynolds number and relaxing/contracting parameters are investigated. Mathematical modeling is undertaken and numerical results are constructed using a shooting method.

Methods

Consider two-dimensional MHD unsteady laminar incompressible nanofluid flowing in porous coaxial disks of width $2a(t)$ with viscous dissipation and thermal radiation effects. Compared to the force field, the induced magnetic field is believed to be insignificant. It is assumed that there is no applied polarization. Water is taken as the base fluid. Thermal equilibrium exists between base fluid and nanoparticles. The thermophysical properties are shown in Table 1. Permeability of the disks is similar, with time dependent rate $a'(t)$ (shown in Fig. 1). Thermal conductivity is the most vital thermophysical property that influences nanofluid heat transfer rate. In order to explore efficient thermal conductivity of nanofluids, various theoretical models are currently available. Numerous theoretical studies are discussed in the literature to envisage appropriate models for effective viscosity along with thermal conductivity of nanofluids. The Hamilton–Crosser (H-C) model is the most

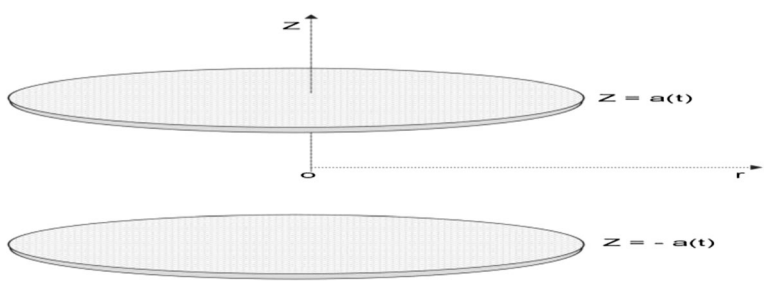

Fig. 1 Physical geometry

common model for effective thermal conductivity of nanofluids and is given by [35]

$$k_{\mathrm{nf}} = k_{\mathrm{f}}\left[\frac{(k_{\mathrm{s}} + (n-1)k_{\mathrm{f}}) - (n-1)\phi(k_{\mathrm{f}} - k_{\mathrm{s}})}{(k_{\mathrm{s}} + (n-1)k_{\mathrm{f}}) + \phi(k_{\mathrm{f}} - k_{\mathrm{s}})}\right]. \quad (1)$$

Here k_{nf} denotes effective thermal conductivity of the nanofluid, k_{f} thermal conductivity of the continuous phase, ϕ the nanoparticles volume fraction, and "n" the shape factor for nanoparticles given by $\frac{3}{\psi}$ where ψ is the sphericity of the nanoparticles and determined by the shape of the nanoparticles [36, 37]. For spherical nanoparticles $\psi = 1$ or $n = 3$ and for cylindrical nanoparticles $\psi = 0.5$ or $n = 6$.

The geometry of the problem recommends that a cylindrical coordinate system may be selected with the origin at the center of the two disks. We take u and w as velocity components in the r and z directions, respectively. The governing equations for the problem, taking into account effects of thermal radiation and viscous dissipation, are as follows:

$$\frac{\partial u}{\partial r} + \frac{u}{r} + \frac{\partial w}{\partial z} = 0, \quad (2)$$

$$\frac{\partial u}{\partial t} + u\frac{\partial u}{\partial r} + w\frac{\partial u}{\partial z} = -\frac{1}{\rho_{\mathrm{nf}}}\frac{\partial p}{\partial r} + \upsilon_{\mathrm{nf}}\left(\frac{\partial^2 u}{\partial r^2} + \frac{1}{r}\frac{\partial u}{\partial r} - \frac{u}{r^2} + \frac{\partial^2 u}{\partial z^2}\right) - \frac{\sigma_{\mathrm{e}} B_0^2}{\rho_{\mathrm{nf}}}u, \quad (3)$$

$$\frac{\partial w}{\partial t} + u\frac{\partial w}{\partial r} + w\frac{\partial w}{\partial z} = -\frac{1}{\rho_{\mathrm{nf}}}\frac{\partial p}{\partial z} + \upsilon_{\mathrm{nf}}\left(\frac{\partial^2 w}{\partial r^2} + \frac{1}{r}\frac{\partial w}{\partial r} + \frac{\partial^2 w}{\partial z^2}\right) - \frac{\sigma_{\mathrm{e}} B_0^2}{\rho_{\mathrm{nf}}}v, \quad (4)$$

$$\frac{\partial T}{\partial t} + u\frac{\partial T}{\partial r} + w\frac{\partial T}{\partial z} = \alpha_{\mathrm{nf}}\left(\frac{\partial^2 T}{\partial r^2} + \frac{1}{r}\frac{\partial T}{\partial r} + \frac{\partial^2 T}{\partial z^2}\right) + \frac{\mu_{\mathrm{nf}}}{(\rho c_p)_{\mathrm{nf}}}\left(\frac{\partial u}{\partial z}\right)^2 - \frac{1}{(\rho c_{\mathrm{p}})_{\mathrm{nf}}}\left(\frac{\partial q_{\mathrm{r}}}{\partial z}\right), \quad (5)$$

$$\frac{\partial C}{\partial t} + u\frac{\partial C}{\partial r} + w\frac{\partial C}{\partial z} = D\left(\frac{\partial^2 C}{\partial r^2} + \frac{1}{r}\frac{\partial C}{\partial r} + \frac{\partial^2 C}{\partial z^2}\right), \quad (6)$$

where σ_{e} is the electrical conductivity, B_0 is the strength of the magnetic field, p is the pressure, T is the temperature, C is the mass concentration, D is the mass diffusion coefficient, α_{nf} is the thermal diffusivity, ρ_{nf} is the density, and υ_{nf} is the kinematics viscosity of the nanofluid, are given by

$$\upsilon_{\mathrm{nf}} = \frac{\mu_{\mathrm{nf}}}{\rho_{\mathrm{nf}}},\ \mu_{\mathrm{nf}} = \frac{\mu_{\mathrm{f}}}{(1-\phi)^{2.5}},\ \rho_{\mathrm{nf}} = (1-\phi)\rho_{\mathrm{f}} + \phi\rho_{\mathrm{s}},\ \alpha_{\mathrm{nf}} = \frac{k_{\mathrm{nf}}}{(\rho c_{\mathrm{p}})_{\mathrm{nf}}},\ (\rho c_{\mathrm{p}})_{\mathrm{nf}} = (1-\phi)(\rho c_{\mathrm{p}})_{\mathrm{f}} + \phi(\rho c_{\mathrm{p}})_{\mathrm{s}}, \quad (7)$$

Table 2 Effect of Tr on heat and mass transfer rate for $Pr = 6.2$, $M = Br = Re = 1$

a	M	Re	$(1-\phi)^{-2.5}\lvert f''(-1)\rvert$	$\left(1+\frac{4Tr}{3}\right)\frac{K_{nf}}{K_f}\lvert\theta'(-1)\rvert$	$\lvert\chi'(-1)\rvert$
1	1	−2	1.7367	1.1646	0.1347
		−1	1.6334	0.3773	0.2222
		1	2.2353	0.8153	0.5372
		2	4.9848	6.6129	0.7577
	3	−2	1.8443	1.2178	0.1353
		−1	1.8065	0.3895	0.2230
		1	2.7800	0.7700	0.5347
		2	5.5159	6.6559	0.7537
	5	−2	1.9515	1.2731	0.1361
		−1	1.9750	0.4040	0.2237
		1	3.2411	0.7600	0.5326
		2	5.9635	6.7693	0.7504
−1	1	−2	2.7219	2.6761	0.2813
		−1	3.5276	0.7798	0.4696
		1	7.5649	0.9732	0.9592
		2	8.3928	7.2856	1.0967
	3	−2	2.1821	1.6000	0.2405
		−1	3.7173	0.7956	0.4704
		1	7.7960	1.0016	0.9585
		2	7.1262	5.3874	1.0068
	5	−2	1.8227	1.0240	0.2448
		−1	3.8999	0.8133	0.4712
		1	8.0133	1.0304	0.9578
		2	5.7594	3.5199	1.0006
		Tr	ϕ	$\left(1+\frac{4Tr}{3}\right)\frac{K_{nf}}{K_f}\lvert\theta'(-1)\rvert$	$\lvert\chi'(-1)\rvert$
		0.1	0	3.8648	0.5343
			0.05	3.7882	0.5357
			0.07	3.7766	0.5363
			0.1	3.7751	0.5372
		0.5	0	2.6586	0.5343
			0.05	2.6138	0.5357
			0.07	2.6081	0.5363
			0.1	2.6003	0.5372
		1	0	1.3910	0.5343
			0.05	0.7962	0.5357
			0.07	0.8011	0.5363
			0.1	0.8153	0.5372

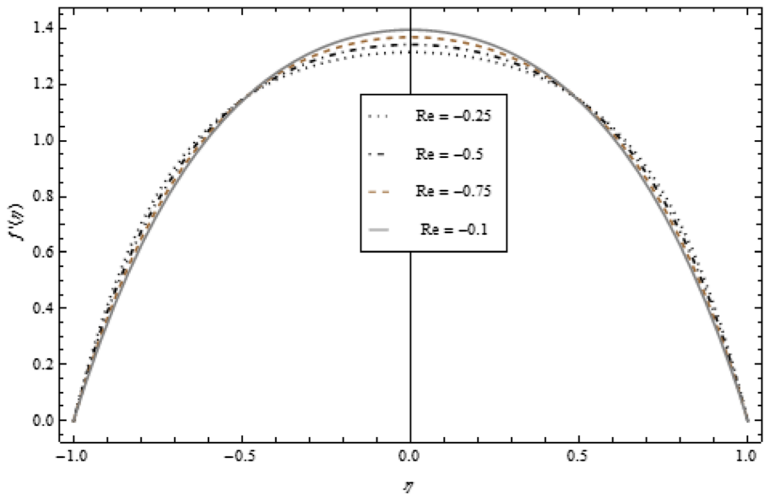

Fig. 2 Velocity profile under the influence of Re < 0 for $\{a = 1, M = Br = Tr = Sc = 1, \phi = 0.1\}$

where ρ_s and ρ_f are, respectively, the densities of the solid fractions and fluid and $(\rho c_p)_{nf}$ is the heat capacitance of the nanofluid. The boundary conditions are

$$\begin{aligned} &u = 0; v = -Aa'(t), \text{at} z = -a(t) \text{when} T = T_1 \text{and} C = C_1, \\ &u = 0; v = Aa'(t), \text{at} z = a(t) \text{ when} T = T_1 \text{and} C = C_1. \end{aligned} \quad (8)$$

Here, A is a measure of the disk permeability and the dash denotes derivative w.r.t. time t.

Using the Rosseland approximation for radiation, the radiative heat flux is

$$q_r = \frac{-4\sigma_{sB}}{3m_0}\left(\frac{\partial T^4}{\partial z}\right), \quad (9)$$

where σ_{sB} is the Stefan-Boltzman constant and m_0 is the mean absorption coefficient. Assume that difference in temperature within the flow is such that T^4 can be expressed as a linear combination of temperature. Now, expand T^4 in Taylor series about T_2 as follows:

$$T^4 = {T_2}^4 + 4{T_2}^3(T - T_2) + 6{T_2}^2(T - T_2)^2 + \ldots \quad (10)$$

Neglect higher order terms beyond the first degree $(T - T_2)$ as follows:

$$T^4 \cong -3{T_2}^4 + 4{T_2}^3 T. \quad (11)$$

By substituting Eq. (11) into Eq. (9) we obtain:

$$\frac{\partial q_r}{\partial z} = \frac{-16\sigma_{sB}{T_2}^3}{3m_0}\left(\frac{\partial^2 T}{\partial z^2}\right). \quad (12)$$

Now using Eq. (12) in Eq. (5), we obtain

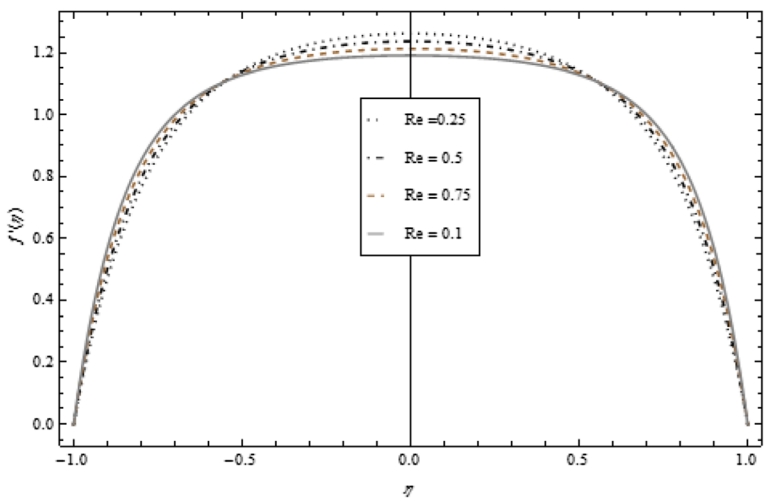

Fig. 3 Velocity profile under the influence of Re > 0 for $\{a = 1, M = Br = Tr = Sc = 1, \phi = 0.1\}$

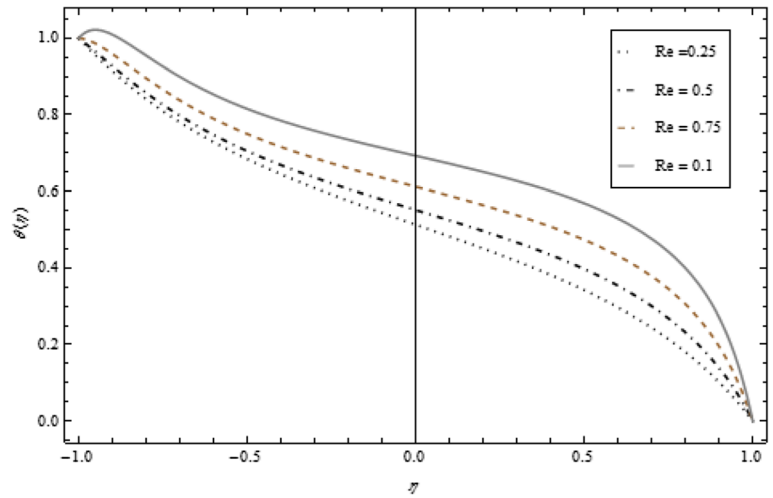

Fig. 4 Temperature profile under the influence of Re > 0 for $\{a = 1, M = Br = Tr = Sc = 1, \phi = 0.1\}$

$$\frac{\partial T}{\partial t} + u\frac{\partial T}{\partial r} + w\frac{\partial T}{\partial z} = \alpha_{\mathrm{nf}}\left(\frac{\partial^2 T}{\partial r^2} + \frac{1}{r}\frac{\partial T}{\partial r} + \frac{\partial^2 T}{\partial z^2}\right) + \frac{\mu_{\mathrm{nf}}}{(\rho c_{\mathrm{p}})_{\mathrm{nf}}}\left(\frac{\partial u}{\partial z}\right)^2 + \frac{1}{(\rho c_{\mathrm{p}})_{\mathrm{nf}}}\frac{16\sigma_{\mathrm{sB}}T_2^{\,3}}{3m_0}\left(\frac{\partial^2 T}{\partial z^2}\right). \tag{13}$$

After removing the pressure term from the governing equations, we introduce the following similarity transformation:

$$\eta = za^{-1},\ u = -rv_{\mathrm{f}}a^{-2}F_{\eta}(\eta,t),\ w = 2v_{\mathrm{f}}a^{-1}F(\eta,t),\quad \theta(\eta) = \frac{T-T_2}{T_1-T_2}, \chi(\eta) = \frac{C-C_2}{C_1-C_2}. \tag{14}$$

The dimensions of v_{f} are $[L^2T^{-1}]$, those of both u and w are $[LT^{-1}]$, and finally $[L]$ is the dimension of each of a and r, which when used in Eq. (14), give $F\left(=\frac{aw}{2v_{\mathrm{f}}}\right)$ and $F_{\eta}\left(=-\frac{a^2u}{rv_{\mathrm{f}}}\right)$ as the two dimensionless velocities in the axial and radial directions, respectively, between the porous disks. On the other hand, $\theta(\eta)$ and $\chi(\eta)$ being the ratio of two quantities having the same units is also dimensionless.

The transformation given in Eq. (14) leads to:

$$\frac{v_{\mathrm{nf}}}{v_{\mathrm{f}}}F_{\eta\eta\eta\eta} + \alpha\left(3F_{\eta\eta} + \eta F_{\eta\eta\eta}\right) - 2FF_{\eta\eta\eta} - \frac{a^2}{v_{\mathrm{f}}}F_{\eta\eta t} - \frac{\rho_{\mathrm{f}}}{\rho_{\mathrm{nf}}}MF_{\eta\eta} = 0, \tag{15}$$

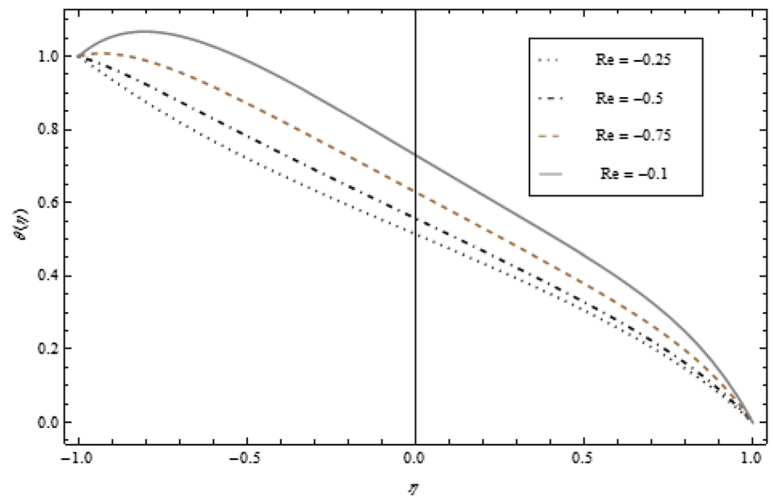

Fig. 5 Temperature profile under the influence of Re < 0 for $\{a = 1, M = Br = Tr = Sc = 1, \phi = 0.1\}$

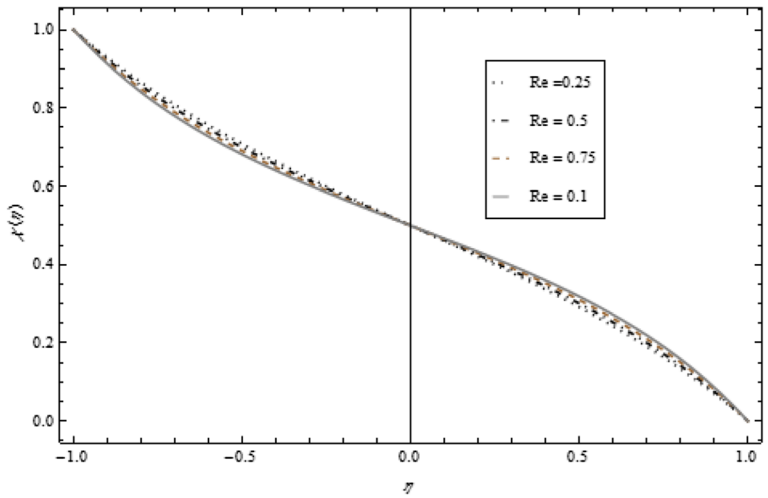

Fig. 6 Mass Transfer profile under the influence of Re > 0 for $\{a = 1, M = Br = Tr = Sc = 1, \phi = 0.1\}$

$$(1 + (4/3)Tr)\theta_{\eta\eta} + \frac{\upsilon_f}{\alpha_{nf}}(\eta\alpha - 2F)\theta_\eta + \left((1-\phi)^{-2.5}F_{\eta\eta}{}^2\right)E_c P_r\left(\frac{k_f}{k_{nf}}\right) - \frac{a^2}{\alpha_{nf}}\theta_t = 0, \tag{16}$$

$$\frac{D}{\upsilon_f}\chi_{\eta\eta} + (\eta\alpha - 2F)\chi_\eta - a^2\chi_t = 0, \tag{17}$$

with boundary conditions:

$$\begin{aligned} &F = -\mathrm{Re};\ F_\eta = 0,\ \text{at}\,\eta = -1\,\text{when}\,\theta = 1\,\text{and}\,\chi = 1,\\ &F = \mathrm{Re};\ F_\eta = 0,\ \text{at}\,\eta = 1\,\text{when}\,\theta = 0\,\text{and}\,\chi = 0. \end{aligned} \tag{18}$$

Here T_1 and T_2 (with$T_1 > T_2$) are the fixed temperatures of the lower and upper disks, respectively, $\alpha = \frac{a\,a'(t)}{\upsilon_f}$ is the wall expansion ratio, $\mathrm{Re} = \frac{A a\, a'}{2\upsilon_f}$ is the permeability Reynolds number, $M = \frac{\sigma_e B_0^2 a^2}{\mu_f}$ is the magnetic parameter, $P_r = \frac{(\mu c_p)_f}{k_f}$ is the Prandtl number, $Ec = \frac{(r\upsilon_f)^2}{a^4(T_1 - T_2)(c_p)_f}$ is the Eckert number and $Br = \mathrm{Pr}$. Ec is the Brinkman number.

It is worth-mentioning here that the continuity Eq. (1) is identically satisfied, that is, the proposed velocity is compatible with Eq.(1) and, thus, represents possible fluid motion.

Finally, we set $f = \frac{F}{\mathrm{Re}}$, and consider the case (following Kashif et al. [15]), we take $Aa'(t) = \upsilon_w$, and then the permeable Reynolds number becomes $\mathrm{Re} = \frac{a(t)\upsilon_w}{\upsilon_f}$. When α is a constant $f = f(\eta)$, $\theta = \theta(\eta)$ and $\chi = \chi(\eta)$ which leads to $\chi_t = 0$, $\theta_t = 0$, and $f_{\eta\eta\,t} = 0$. Thus, we have

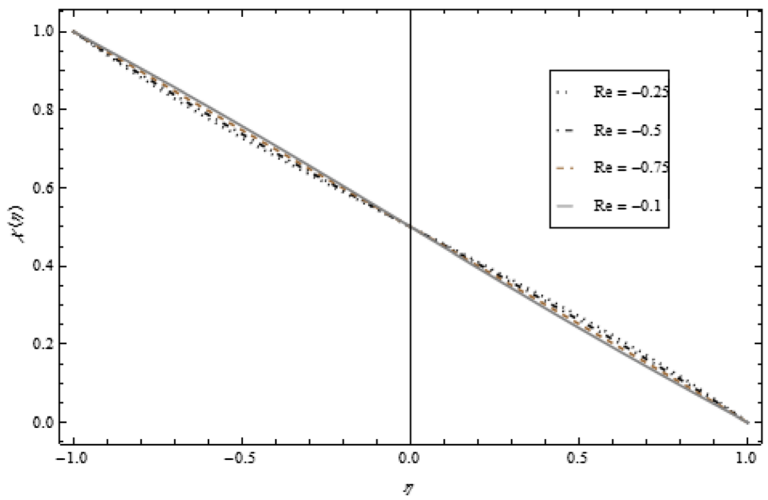

Fig. 7 Mass profile under the influence of Re < 0 for $\{a = 1, M = Br = Tr = Sc = 1, \phi = 0.1\}$

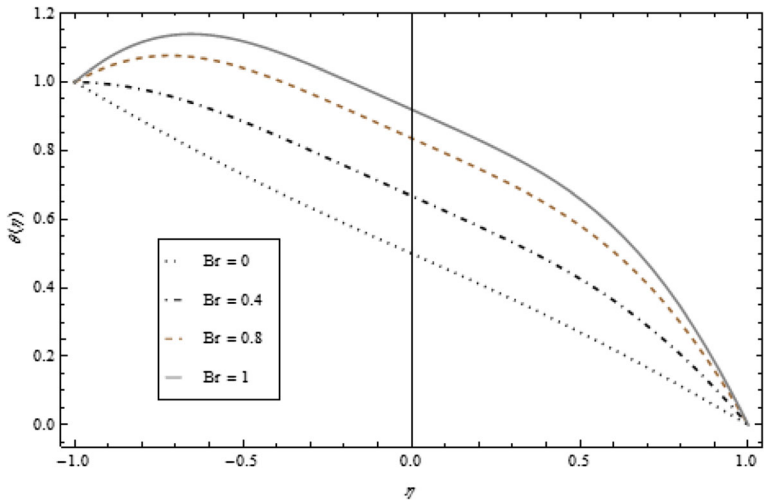

Fig. 8 Temperature profile under the influence of *Br* for $\{a = 1, M = Tr = Sc = 1, \phi = 0.1\}$

$$\frac{v_{nf}}{v_f} f_{\eta\eta\eta\eta} + \alpha\left(3f_{\eta\eta} + \eta f_{\eta\eta\eta}\right) - 2\mathrm{Re}f f_{\eta\eta\eta} - \frac{\rho_f}{\rho_{nf}} M f_{\eta\eta} = 0, \quad (19)$$

$$(1 + 4Tr/3)\theta_{\eta\eta} + \frac{v_f}{\alpha_{nf}}(\eta\alpha - 2\mathrm{Re}f)\theta_\eta + \mathrm{Re}^2\left((1-\phi)^{-2.5} f_{\eta\eta}{}^2\right) Br\left(\frac{k_f}{k_{nf}}\right) = 0, \quad (20)$$

$$\chi_{\eta\eta} + Sc(\eta\alpha - 2\mathrm{Re}f)\chi_\eta = 0, \quad (21)$$

$$f = -1; f_\eta = 0, \text{ at } \eta = -1 \text{ when } \theta = 1 \text{ and } \chi = 1,$$
$$f = 1; f_\eta = 0, \text{ at } \eta = 1 \text{ when } \theta = 0 \text{ and } \chi = 0. \quad (22)$$

The physical quantities of engineering applications are the skin friction coefficient C_f, the Nusselt number Nu, and the Sherwood number Sh, which can be written as

$$C_f = \frac{2\tau_{rz}}{\rho_f u^2},\ Nu = \frac{rq_w}{K_f(T_1 - T_2)},\ Sh = \frac{rq_m}{D(C_1 - C_2)},$$

where τ_{rz} is the disk radial shear stress and q_w and q_m are the wall heat and mass flux of the lower disk, respectively. These parameters are given by

$$\tau_{rz} = \mu_{nf}\left(\frac{\partial u}{\partial z}\right)_{z=-1},\ q_w = q_r - K_{nf}\left(\frac{\partial T}{\partial z}\right)_{z=-1},\ q_m = -D\left(\frac{\partial C}{\partial z}\right)_{z=-1}. \quad (23)$$

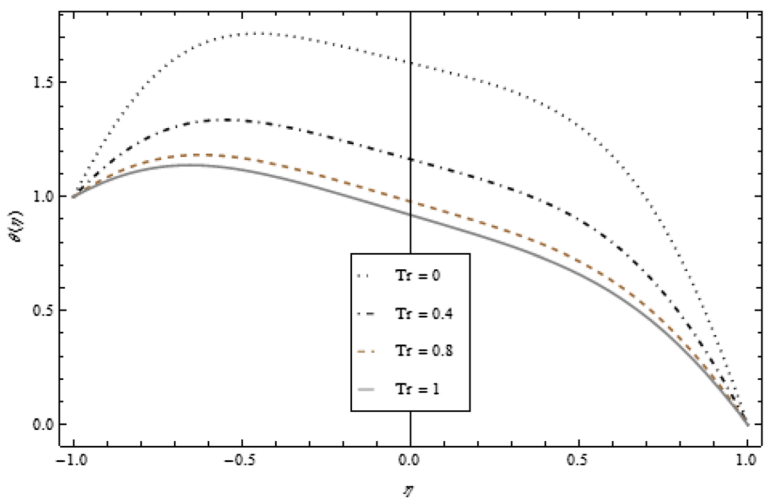

Fig. 9 Temperature profile under the influence of *Tr* for $\{a = 1, M = Br = Sc = 1, \phi = 0.1\}$

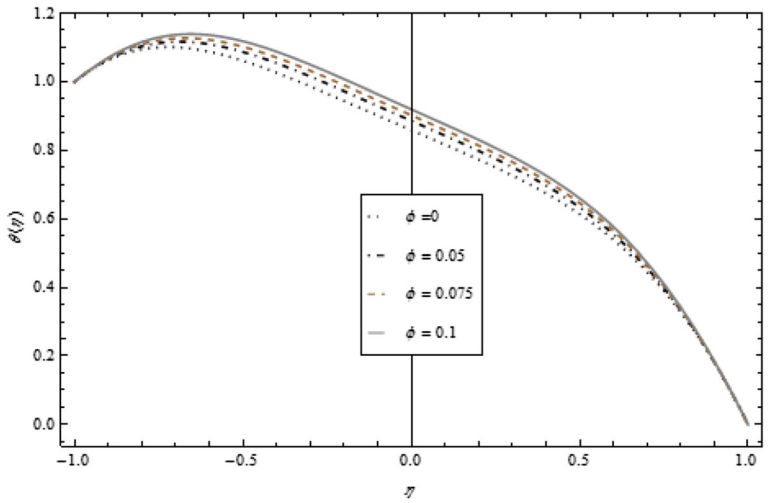

Fig. 10 Temperature profile under the influence of ϕ for $\{a = 1, M = Br = Tr = Sc = 1\}$

Numerical Solution

A numerical technique known as the "shooting method" based on Runge-Kutta fourth order is applied and is bound to the system of nonlinear coupled Eqs. (20)–(22) with boundary conditions Eq. (23). Before applying the numerical method, we convert the governing DEs into a system of first-order ordinary differential equations (ODEs).

A common methodology is to compile the nonlinear ODEs as a system of first order initial value problems as follows:

Put $f' = a, f'' = b, f''' = c$, $\theta' = d$, $\chi' = e$, in Eqs. (20)–(22), then we have $f' = a, a' = b, b' = c$,

and

$$\left.\begin{aligned} c' &= -\frac{\upsilon_f}{\upsilon_{nf}}[\alpha(3b+\eta c)-(Mb+2\mathrm{Re})fc] \\ d' &= -(1+4Tr/3)^{-1}\left[(\eta\alpha-2\mathrm{Re}f)c+\mathrm{Re}^2(1-\phi)^{-2.5}.b^2\right)Br.\frac{K_f}{K_{nf}}\Big] \\ e' &= -Sc(\eta\alpha-2\mathrm{Re}f)e \end{aligned}\right\}. \tag{24}$$

With the following obligatory boundary conditions:

$$\begin{aligned} f(-1) = -1, a(-1) = -1, \theta(-1) = 1, \chi(-1) \\ = 1,\ b(-1) = \Theta 1, c(-1) = \Theta 2, d(-1) \\ = \Theta 3, e(-1) = \Theta 4. \end{aligned} \tag{25}$$

Here, $\Theta 1, \Theta 2, \Theta 3$, and $\Theta 4$ are missing initial conditions. Therefore, at this stage we apply a shooting method which is an accurate and effective way to

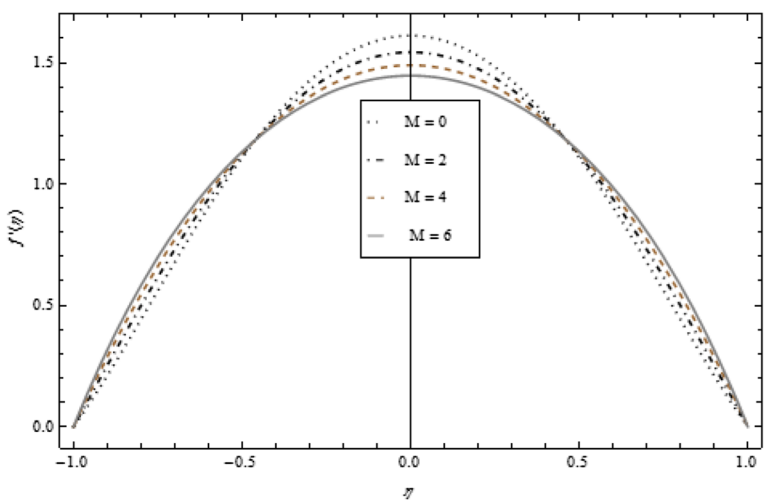

Fig. 11 Velocity profile under the influence of M for $\{a = 1, Br = Tr = Sc = 1, \phi = 0.1\}$

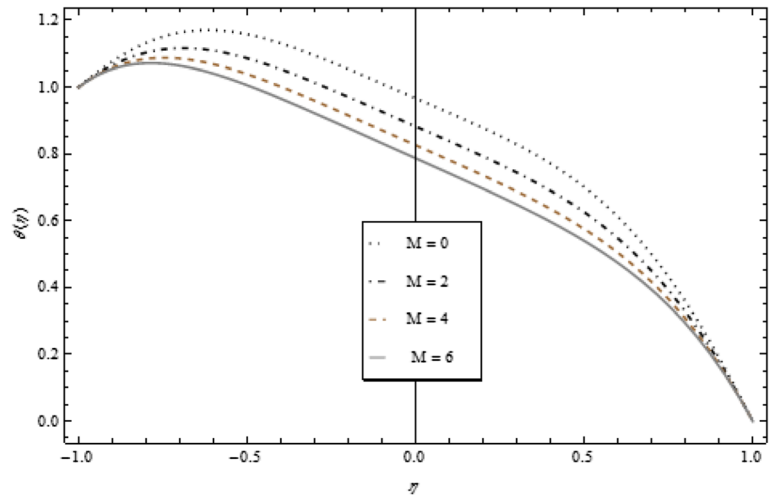

Fig. 12 Temperature profile under the influence of M for $\{a = 1, Br = Tr = Sc = 1, \varphi = 0.1\}$

determine the unknown initial conditions with the least computation. It is imperative to note that the missing initial conditions are computed until the solution satisfies the boundary conditions $f(1) = 1$, $a(1) = 0, \theta(1) = 0, \chi(1) = 0$.

Results and Discussion

Physical quantities we take into account are the skin friction coefficient, the heat and mass transfer rates at the lower disk which are proportionate to $(1-\phi)^{-2.5}|f''(-1)|$, $\left(1+\frac{4Tr}{3}\right)\frac{K_{nf}}{K_f}\left|\theta'(-1)\right|$ and $|\chi'(-1)|$, respectively. The parameters that govern this study are as follows: Re is the permeable Reynolds number, ϕ is the nanoparticle volume fraction parameter, M is the magnetic parameter, α is the wall expansion ratio, Br is the Brinkman number, Sc is the Schmidt number, and Tr is the thermal radiation parameter. Note that $\alpha < 0$ or $\alpha > 0$ according to the case when the disks are contracting or relaxing, while $\mathrm{Re} < 0$ for suction and $\mathrm{Re} > 0$ for injection.

In Table 1, we indicate how the abovementioned parameters affect shear stress, heat, and mass transfer rate at the lower disk, whether the disks are relaxing or contracting. For the relaxing case, M escalates the shear stress along with the heat transfer rate for suction as well as for injection, but M drops the mass transfer rate in the case of suction and rises in the case of injection. However, in the contracting case, suction drops the heat and mass transfer. But heat transfer rate significantly escalates for two cases of the permeable Reynolds number Re. Table 2 explains the behavior of the heat and mass transfer rate under the effect of thermal radiation in the

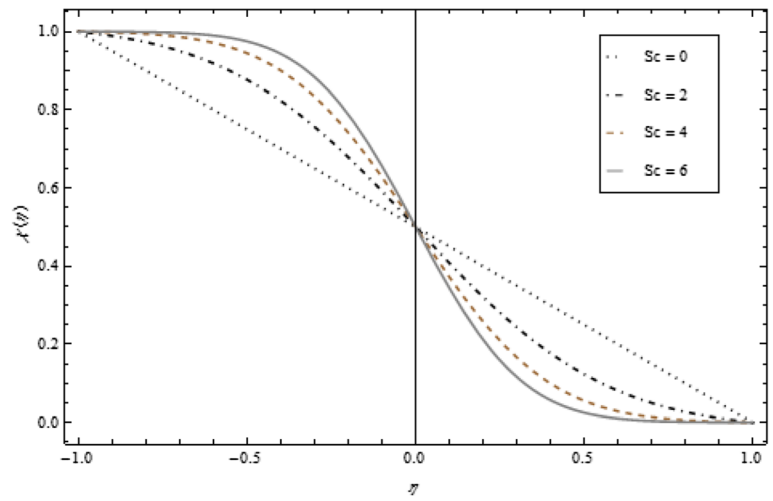

Fig. 13 Mass transfer profile under the influence of Sc for $\{a = 1, M = Br = Tr = 1, \phi = 0.1\}$

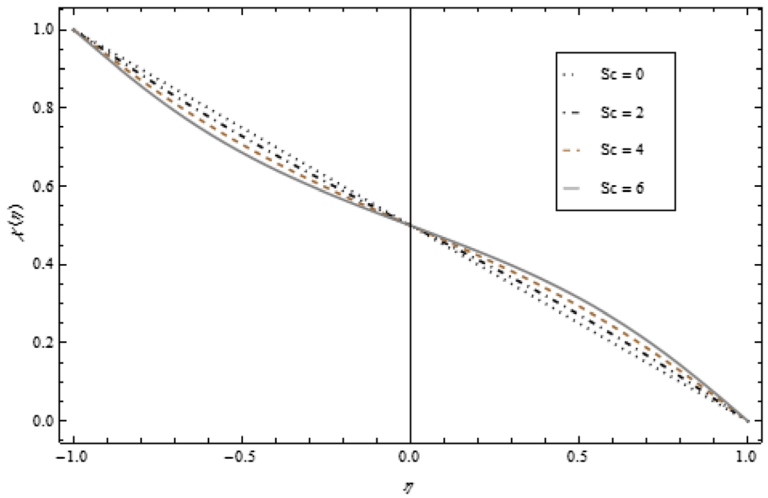

Fig. 14 Mass transfer profile under the influence of *Sc* for $\{\alpha = 1, M = Br = Tr = 1, \mathrm{Re} = -1, \phi = 0.1\}$

presence of nanoparticles. Thermal radiative heat flux reduces the heat transfer rate but the opposite tendency is seen for mass transfer rate.

Figures 2, 3, 4, 5, 6, and 7 depict the behavior of Re on velocity, heat, and mass transfer profiles. In the case of suction, increasing behavior is observed in the center of the disks and decreasing tendency is viewed nearby the lower and upper disks as demonstrated in Fig. 2.

Thickness of the momentum boundary layer is an increasing function of $\mathrm{Re} < 0$. Figure 3 demonstrates quite the opposite trend for the injection case. Heat transfer profiles significantly increase across the whole domain of the disks for suction and injection cases as shown in Figs. 4 and 5. Injection increases the mass transfer profile nearby the upper disk and decreases nearby the lower disk. The reverse tendency is noted in the case of suction as shown in Figs. 6 and 7. Brinkman number *Br* is vital phenomenon for heat conduction in a porous surface and has a considerable effect on heat transfer. Due to the existence of metallic spherical nanoparticles, heat transfer is an increasing function of *Br* and a decreasing function of thermal radiative heat flux with injection as given in Figs. 8 and 9. Heat transfer escalates with increase in nanoparticles volume fraction as described in Fig. 10. The external magnetic field has a tendency to reduce velocity in the center of the two disks. So for this area, the magnetic field behaves like a drag force which is known as the Lorentz force. This force ultimately reduces the fluid velocity as well as temperature profile as exhibited in Figs. 11 and 12. The thickness of the momentum boundary layer is also a decreasing function of *M*. Figures 13 and 14 demonstrate the behavior of mass transfer profile under the effect of *Sc* the Schmidt number with injection and suction effects, respectively. Basically, *Sc* is the ratio of kinematic viscosity to mass diffusivity coefficient, *Sc* is an increasing function, and then dominant kinematic viscosity function has a significant effect on mass transfer profile. Decreasing function is observed near the upper disk and vice versa exists near the lower disk for the injection case as shown in Fig. 13. For the suction case, the opposite trend is observed in Fig. 14.

Conclusions

In this paper, we undertook a numerical study to explore the mechanism which explains the effects of governing parameters on flow and heat transfer features of laminar, incompressible, unsteady, two-dimensional flow of a nanofluid, which is water-based and contains gold spherical nanoparticles, between two porous coaxial disks that are moving orthogonally. In the case of expanding disks ($\alpha > 0$), heat transfer rate and shear stress at the lower disk escalate with *M* and Re, whereas heat transfer rate falls with ϕ and *Tr*. Moreover, mass transfer rate decreased in the case of suction and increased in the case of injection. As far as contracting disks ($\alpha < 0$) are concerned, shear stress at the disks escalates with *M* and α; however, a reverse impact is found for ϕ and *R*. Furthermore, it is concluded that heat transfer rate rises with *M*, *R*, α, and ϕ.

Abbreviations

DEs: Differential equations; MHD: Magnetohydrodynamic; ODEs: Ordinary differential equations

Acknowledgements

We are very thankful to the Higher Education Commission (HEC) of Pakistan and Air University, Islamabad for providing the research environment and sufficient resources in order to conduct this study.

Authors' Contributions

All authors have equally contributed in this work. All authors read and approved the final manuscript.

Competing Interests
The authors declare that they have no competing interests.

Author details
[1]Department of Computer Science, Air University, Multan Campus, Islamabad, Pakistan. [2]Department of Management Sciences, Air University, Multan Campus, Islamabad, Pakistan. [3]Department of Applied Mathematics and Statistics, Institute of Space Technology, Islamabad, Pakistan.

Received: 12 August 2016 Accepted: 15 October 2016
Published online: 24 October 2016

References

1. Bakier AY (2001) Thermal radiation effect on mixed convection from vertical surface in saturated porous media. Int Commun Heat Mass Transf 28:119–126
2. Damseh RA (2006) Magnetohydrodynamics-mixed convection from radiate vertical isothermal surface embedded in a saturated porous media. J Appl Mech 73:54–59
3. Hossain MA, Takhar HS (1996) Radiation effect on mixed convection along a vertical plate with uniform surface temperature. Heat Mass Transf 31:243–248
4. Zahmatkesh I (2007) Influence of thermal radiation on free convection inside a porous enclosure. Emir J Eng Res 12:47–52
5. Moradi A, Ahmadikia H, Hayat T, Alsaedi A (2013) On mixed convection-radiation interaction about an inclined plate through a porous medium. Int J Therm Sci 64:129–136
6. Pal D, Mondal H (2009) Radiation effects on combined convection over a vertical flat plate embedded in a porous medium of variable porosity. Meccanica 44:133–144
7. Hayat T, Rashid M, Imtiaz M, Alsaedi A (2015) Magneto hydrodynamic (MHD) flow of Cu-water nanofluid due to a rotating disk with partial slip. AIP Adv. doi:10.1063/1.4923380
8. Das SK, Choi SUS, Yu W, Pradet T (2007) Nanofluids: science and technology. Wiley, New York
9. Atif N, Tahir M (2011) Analysis of flow and heat transfer of viscous fluid between contracting rotating disks. Appl Math Model 35:3154–3165
10. Hayat T, Mumtaz S, Ellahi R (2003) MHD unsteady flows due to non-coaxial rotations of a disk and a fluid at infinity. Acta Mech Sin 19:235–240
11. Bachok N, Ishak A, Pop I (2011) Flow and heat transfer over a rotating porous disk in a nanofluid. Physica B 406:1767–1772
12. Sheikholeslami M, Hatami M, Ganji DD (2014) Nanofluid flow and heat transfer in a rotating system in the presence of a magnetic field. J Mol Liq 190:112–120
13. Si X, Zheng L, Xx Z, Xy S (2012) Flow of micropolar fluid between two orthogonally moving porous disks. Appl Math Mech Engl Ed 33:963–974
14. Ashraf M, Anwar KM, Syed KS (2009) Numerical simulation of flow of a micropolar fluid between a porous disk and a non-porous disk. Appl Math Model 33:1933–1943
15. Kashif A, Farooq MI, Zubair A, Ashraf M (2014) Numerical simulation of unsteady water-based nanofluid flow and heat transfer between two orthogonally moving porous coaxial disks. J Theor Appl Mech 52:1033–1046
16. Nikiforov VN (2007) Magnetic induction hyperthermia. Russ Phys J 50:913–924
17. Hatami M, Nouri R, Ganji DD (2013) Forced convection analysis for MHD Al 2O3-water nanofluid flow over a horizontal plate. J Mol Liq 87:294–301
18. Hatami M, Ganji DD (2014) Heat transfer and nanofluid flow in suction and blowing process between parallel disks in presence of variable magnetic field. J Mol Liq 190:159–168
19. Sheikholeslami M, G-Bandpy M, Ellahi R, Hassan M, Soleimani S (2014) Effects of MHD on Cu-water nanofluid flow and heat transfer by means of CVFEM. J Magn Magn Mater 349:188–200
20. Sheikholeslami M, Gorji-Bandpy M, Ganji DD (2012) Magnetic field effects on natural convection around a horizontal circular cylinder inside a square enclosure filled with nanofluid. Int Commun Heat Mass Transf 39:978–986
21. Sheikholeslami M, Gorji-Bandpy M, Ganji DD, Soleimani S (2014) Heat flux boundary condition for nanofluid filled enclosure in presence of magnetic field. J Mol Liq 193:174–184
22. Sheikholeslami M, Soleimani S, Gorji-Bandpy M, Ganji DD, Seyyedi SM (2012) Natural convection of nanofluids in an enclosure between a circular and sinusoidal cylinder in the presence of magnetic field. Int Commun Heat Mass Transf 39:1435–1443
23. Sheikholeslami M, Gorji-Bandpy M (2014) Free convection of ferrofluid in a cavity heated from below in the presence of an external magnetic field. Powder Technol 256:490–498
24. Sheikholeslami M, Vajravelu K, Rashidi MM (2016) Forced convection heat transfer in a semi annulus under the influence of a variable magnetic field. Int J Heat Mass Transf 92:339–348
25. Sheikholeslami M, Gorji-Bandpy M, Ganji DD, Rana P, Soleimani S (2014) Magnetohydrodynamic free convection of Al_2O_3–water nanofluid considering Thermophoresis and Brownian motion effects. Comput Fluids 94:147–160
26. Sheikholeslami M, Ganji DD, Javed MY, Ellahi R (2015) Effect of thermal radiation on magnetohydrodynamics nanofluid flow and heat transfer by means of two phase model. J Magn Magn Mater 374:36–43
27. Hayat T, Muhammad T, Alsaedi A, Alhuthali MS (2015) Magneto hydrodynamic three-dimensional flow of viscoelastic nanofluid in the presence of nonlinear thermal radiation. J Magn Magn Mater 385:222–229
28. Hayat T, Rashid M, Imtiaz M, Alsaedi A (2015) Magnetohydrodynamic flow of Cu-water nanofluid due to a rotating disk with partial slip. AIP Adv doi. doi:10.1063/1.4923380
29. Hayat T, Abbasi FM, Al-Yami M, Monaquel S (2014) Slip and Joule heating effects in mixed convection peristaltic transport of nanofluid with Soret and Dufour effects. J Mol Liq 194:93–99
30. Rashidi MM, Ganesh NV, Hakeem AKA, Ganga B (2014) Buoyancy effect on MHD flow of nanofluid over a stretching sheet in the presence of thermal radiation. J Mol Liq 198:234–238
31. Mehrez Z, El Gafsi A, Belghith A, Le Quéré P (2015) MHD effects on heat transfer and entropy generation of nanofluid flow in an open cavity. J Magn Magn Mater 374:214–224
32. Mabood F, Khan WA, Ismail AIM (2015) MHD boundary layer flow and heat transfer of nanofluids over a nonlinear stretching sheet: a numerical study. J Magn Magn Mater 374:569–576
33. Abbasi FM, Shehzad SA, Hayat T, Alsadi A, Obid MA (2015) Influence of heat and mass flux conditions in hydromegnetic flow of Jeffrey nanofluid. AIP Adv doi. doi:10.1063/1.4914549
34. Shehzad SA, Abbasi FM, Hayat T, Alsaadi F (2014) MHD mixed convective peristaltic motion of nanofluid with joule heating and thermophoresis effects. PLoS One 9(11):e111417
35. Hamilton RL, Crosser OK (1962) Thermal conductivity of heterogeneous two component systems. Ind Eng Chem Fundamen 1:187–191
36. Ali K, Akbar Qureshi MZ, Iqbal FM, Ashraf M (2014) Numerical simulation of heat and mass transfer in unsteady nanofluid between two orthogonally moving porous coaxial disks. AIP Adv 4:107113. doi:10.1063/14897947
37. Akbar Qureshi MZ, Ashraf M, Iqbal MF, Ali K (2016) Heat and mass transfer analysis of unsteady MHD nanofluid flow through a channel with moving porous walls and medium. AIP Adv 6:045222. doi:10.1063/1495440